

Structural Basis of Pilus Subunit Recognition by the PapD Chaperone

Meta J. Kuehn, Derek J. Ogg, Jan Kihlberg, Lynn N. Slonim, Katarina Flemmer, Terese Bergfors, Scott J. Hultgren*

The assembly of different types of virulence-associated surface fibers called pili in Gram-negative bacteria requires periplasmic chaperones. PapD is the prototype member of the periplasmic chaperone family, and the structural basis of its interactions with pilus subunits was investigated. Peptides corresponding to the carboxyl terminus of pilus subunits bound PapD and blocked the ability of PapD to bind to the pilus adhesin PapG *in vitro*. The crystal structure of PapD complexed to the PapG carboxyl-terminal peptide was determined to 3.0 Å resolution. The peptide bound in an extended conformation with its carboxyl terminus anchored in the interdomain cleft of the chaperone via hydrogen bonds to invariant chaperone residues Arg⁸ and Lys¹¹². Main chain hydrogen bonds and contacts between hydrophobic residues in the peptide and the chaperone stabilized the complex and may play a role in determining binding specificity. Site-directed mutations in Arg⁸ and Lys¹¹² abolished the ability of PapD to bind pilus subunits and mediate pilus assembly *in vivo*, an indication that the PapD-peptide crystal structure is a reflection of at least part of the PapD-subunit interaction.

Molecular chaperones are vital components of all living cells, prokaryotic and eukaryotic. Chaperones serve many cellular functions, including folding, import, and export of proteins in various cellular compartments (1). At present, little is known about the molecular recognition motifs of chaperones. Bacterial cytoplasmic chaperones such as DnaK, GroEL, BiP, and SecB bind to various groups of unfolded target proteins in a sequence independent manner (1). It has been suggested that DnaK binds mainly via the peptide backbone of the target (2). GroEL (3) and BiP (4) have been shown to selectively bind polypeptides containing hydrophobic and aliphatic residues, whereas SecB (5) preferentially recognizes positively charged side chains.

Chaperones also exist in the periplasm of Gram-negative bacteria and are required for the assembly of many virulence-associated, adhesive surface structures called pili (Table 1) (6–10). Pili are usually heteropolymeric fibers that mediate attachment to eukaryotic cells, an important early event in bacterial infections. P pili have been associated with virulence in pyelonephritic *Escherichia coli* and are assembled by the periplasmic chaperone PapD. The 11

genes organized in the pyelonephritis-associated pilus (pap) gene cluster required for P pilus production have been cloned, sequenced, and characterized (6). P pili are composite fibers consisting of a thin heteropolymeric tip fibrillum joined end to end to a thick pilus rod (11). The tip fibrillum is a linear fiber composed of four specialized subunits, PapG, PapF, PapE, and PapK. PapG is a bacterial adhesin that mediates binding to the Gal α (1→4)Gal receptor present in the globoseries of glycolipids in the kidney (6). PapF is an adaptor protein that joins PapG to PapE (12). The bulk of the tip fibrillum consists of repeating subunits of PapE, which

is joined to the homopolymeric helical rod by way of the PapK adaptor protein (11, 12). The rod consists of repeating subunits of PapA arranged in a right-handed helix (13) anchored to the bacterial cell by PapH (14). PapD binds to each of the pilus subunit types as they are translocated across the cytoplasmic membrane and escorts them in assembly-competent, native-like conformations through the periplasm to outer membrane assembly sites composed of PapC (6, 15, 16). PapC has been termed a molecular usher (17) because it receives chaperone subunit complexes and incorporates, or ushers, the subunits from the chaperone complex into the growing pilus in a defined order.

The three-dimensional structure of PapD has been solved and refined to a 2.0 Å resolution (18, 19). PapD consists of two globular domains positioned such that the overall shape of the molecule resembles a boomerang with a cleft between the two domains. Each domain is a β -barrel structure formed by two antiparallel β -pleated sheets with a topology similar to that of an immunoglobulin fold. Eleven periplasmic proteins involved in the assembly of cell surface structures in pathogenic bacteria have been found that have significant homology to PapD (Table 1) (7, 10). A structural alignment between PapD and several periplasmic chaperones suggested that they have a similar immunoglobulin-like structure to PapD and revealed invariant, highly conserved and variable residues within this protein family (7). Most conserved residues seem to participate in maintaining the overall structure and orientation of the domains toward one another. However, site-directed mutagenesis has shown that invariant and conserved residues in the PapD cleft form at least part of the pilus subunit binding site (20).

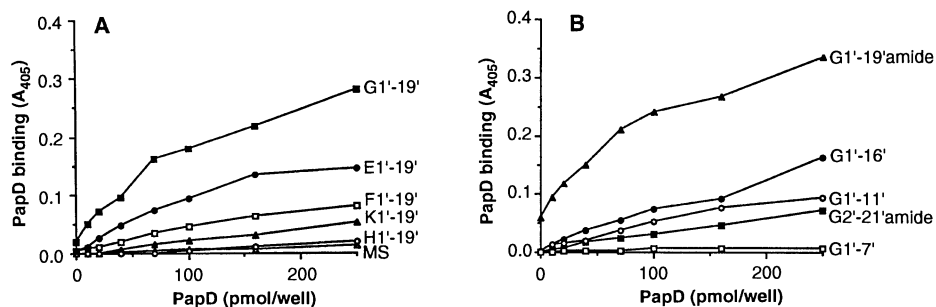


Fig. 1. PapD binds to pilus subunit-related peptides coated in ELISA microtiter plates and in solution. (A and B) The peptides described in Table 2 were coated on microtiter wells and tested for their ability to bind to PapD in an ELISA (24). Water-insoluble peptides were coated to wells in 2.5 percent acetic acid, which had no effect on the binding of G1'-19' to PapD in this assay. Each graph represents the average of duplicate wells. (C) The ability of a 25-times molar excess of the water-soluble peptides to inhibit binding of 100 pmol per well of PapD to G1'-19'-coated wells was tested (25). The percent inhibition represents the percent reduction of PapD binding in the presence of the peptide and is the average of two experiments performed in duplicate.

M. J. Kuehn, L. N. Slonim, and S. J. Hultgren are in the Department of Molecular Microbiology, Washington University, Box 8230, St. Louis, MO 63110. D. J. Ogg is in the Protein Structure Laboratory, Symbicom AB, Glunten, S-751 83, Uppsala, Sweden. J. Kihlberg and K. Flemmer are in the Department of Organic Chemistry 2, University of Lund, Box 124, S-221 00 Lund, Sweden. T. Bergfors is in the Department of Molecular Biology, Uppsala University, Uppsala, Sweden.

*To whom correspondence should be addressed.

Since the subunit-binding cleft of PapD is highly conserved among the members of the chaperone family, the site recognized on the pilus subunits was predicted to contain conserved features (20). A characteristic of pilus proteins assembled by PapD-like chaperones is their conserved COOH-terminal sequence (Table 1) (21). This region generally contains alternating hydrophobic-hydrophilic residues, and also a tyrosine and a glycine at positions 2 and 14 from the COOH-terminus, respectively (21, 22). This region may be part of a site recognized by the chaperone since deletion of the 14 COOH-terminal residues of PapG abolished the formation of the PapD-PapG complex in vivo (16).

We have now discovered that PapD specifically binds synthetic peptides corresponding to the conserved COOH-termini of the P pilus subunits. We determined the x-ray crystal structure of PapD in complex with a COOH-terminal PapG peptide in order to investigate the molecular basis of the PapD-peptide interaction. Site-direct-

ed mutagenesis of PapD confirmed that invariant cleft residues that hydrogen-bonded to the peptide in the crystal were critical for chaperone-subunit interactions in vivo. These investigations have revealed features by which periplasmic chaperones recognize their subunits and mediate pilus assembly.

Binding of the PapD chaperone to COOH-terminal peptides from pilus subunits. To investigate the role of the conserved COOH-termini of the pilus subunits in chaperone binding we used synthetic peptides corresponding to the 19 residues at the COOH-terminus of P pilus subunit proteins PapG (G1'-19'), PapE (E1'-19'), PapF (F1'-19'), PapK (K1'-19'), and PapH (H1'-19') (23) (Table 2). The residues in the peptides were numbered starting with the COOH-terminal residue as 1', and ending with the NH₂-terminal residue, thereby maintaining the COOH-terminus as a point of reference. We used an enzyme-linked immunosorbent assay (ELISA) (24)

to determine the ability of PapD to bind to each of the peptides that were immobilized by coating in wells of microtiter plates (Fig. 1, A and B).

PapD bound well to the wild-type PapG 19-residue peptide (G1'-19'), moderately to the corresponding PapE, PapF, and PapK peptides, and not at all to the PapH peptide or a random, hydrophobic peptide (MS) (Fig. 1A). These results suggested that the PapD chaperone recognizes PapG, PapE, PapF, and PapK in part by binding to the COOH-terminus of these subunits. The inability of PapD to interact with the PapH peptide is not well understood but may suggest that PapD binds differently to PapH, possibly because of its function as a polymerization terminator (14).

To determine the minimum length of peptides required for PapD binding, we synthesized a series of PapG peptides shortened to different degrees at the NH₂-terminus (G1'-16', G1'-11', G1'-7', G1'-4') (Table 2). The affinity of PapD for the immobilized PapG peptides decreased as the length of the peptides decreased until virtually no binding was detected to the immobilized G1'-7' peptide (Fig. 1B). However, the G1'-7' peptide may have been too short to permit simultaneous binding to both the plastic wells and PapD. We therefore tested the ability of the soluble peptides to bind PapD in solution and to inhibit the binding of PapD to the immobilized G1'-19' peptide (25). The G1'-7' and G1'-19' peptides inhibited binding of PapD to G1'-19' peptide-coated wells (Fig. 1C). In contrast, the control MS peptide and the G1'-4' peptide were unable to inhibit PapD binding (Fig. 1C). These experiments revealed that even a short peptide consisting

Table 1. Periplasmic chaperone family and conserved features of COOH-terminal amino acid sequences in subunits they assemble in pathogenic bacteria. Boxed positions contain hydrophobic residues in more than 50 percent of the COOH-terminal sequences examined, shaded boxes indicate positions of highly conserved residues. Abbreviations for the amino acid residues are: A, Ala; C, Cys; D, Asp; E, Glu; F, Phe; G, Gly; H, His; I, Ile; K, Lys; L, Leu; M, Met; N, Asn; P, Pro; Q, Gln; R, Arg; S, Ser; T, Thr; V, Val; W, Trp; and Y, Tyr.

Surface structure (Chaperone)	Subunit	Carboxyl terminal sequence			Reference
		30	20	10	
<i>E. coli</i> P pili (PapD)	PapG*	VK TESRLYGE	EGKRK P G E L S	GSMT TMV L S F P	(33)
	PrsG*	L T IGSRLYGE	SSK T Q P G V L S	GSAT LLM I L P	(33)
	PapA†	T A V K K S S A V	G A A V T E G A F S	A V A N F N L T Y Q	(33)
	PapK	Y V V A T P E A L R	T K S V V P G D Y E	A T A T F E L T Y R	(33)
	PapE	L H A K L G Y K G N	M Q N L I A G P F S	A T A T L V A S Y S	(33)
	PapF	T F T S V P F R G	S G I L N G G D E Q	T T A S M S M I Y N	(33)
PapH	L D Y T L R I V R N	G K K L E A G N Y F	A V L G F R V D Y E	(33)	
S pili (SfaE)	SfaS*	T F N L K A R A V S	K G Q V T P G N I S	S V I T V T Y T Y A	(34)
	SfaA†	K I P F Q A V Y Y A	T G K S T P G I A N	A D A T F K V Q Y Q	(35)
Type 1 pili (FimC)	FimH*	L G L T A N Y A R T	G G Q V T A G N V Q	S I I G V T F V Y Q	(36)
	FimA†	T I P F Q A R Y F A	T G A A T P G A A N	A D A T F K V Q Y Q	(37)
K99 pili (FanC)	FanC*†	Q L K K D R A P S	N G G Y K A G V F T	T S A S F L V T Y M	(38)
F17E pili (F17C)	F17G*	V R L Y V K Y V N T	G E G I N P G T V N	G I S T E T F S Y Q	(39)
	F17A†	T L R Y N A Q Y Y A	T G V A T A G D V T	S T V N Y T I A Y Q	(40)
K88 pili (FaeE)	FaeG*†	N G Q T I E A T F N	Q A V T T S T Q W S	A P L N V A I T Y Y	(41)
CS3 pili (CS3-1)	CS3-3	L P L K F I T T E G	N E H L V S G N Y R	A N I T I T S T I K	(42)
<i>K. pneumoniae</i> Type 3 pili (MrkB)	MrkD*	L P L H A R F Y Q Y	A P T T S T G E V E	S H L V F N L T Y D	(43)
	MrkA†	T Y Y V G Y A T S T	P T T V T T G V V N	S Y A T Y E I T Y Q	(44)
<i>H. influenzae</i> pili (HifB)	M43†	P L H F I A Q Y Y A	T N K A T A G K V Q	S S V D F Q I A Y E	(45)
<i>Y. pestis</i> Capsular antigen F1 (Caf1M)	F1	D F F V R S I G S K	G G K L A A G K Y T	D A V T V T V S N Q	(46)
<i>B. pertussis</i> Serotype 2 and 3 Fimbriae (FhaD, FimB)	Fim2†	M R Y L A S Y V K K	N G D V E A S A I T	T Y V G F S V V Y P	(47)
	Fim3†	R Y L A S Y V K K P	K E D V D A A Q I T	S Y V G F S V V Y P	(48)
<i>S. enteritidis</i> SEF14 Fimbriae (SefB)	SefA†	T L N V P V T T F G	K S T L P A G T F T	A T F Y V Q Q Y Q N	(49)

* Adhesin † Major subunit

Table 2. Synthetic COOH-terminal peptides of P pilus subunits. Peptides corresponding to wild-type and modified COOH-terminal sequences of PapG, PapE, PapF, PapK, and PapH were synthesized and purified as described (23). The first letter of the name of the peptide corresponds to the Pap subunit from which the sequence was derived. Water-insoluble peptides were dissolved in 50 percent acetic acid. MS is a random hydrophobic peptide used as a control.

Name	Peptide sequence
	20 10
G1'-19'	NH ₂ -GKRKPGELSGSMTMVLVSFP-COOH
G1'-16'	NH ₂ -KPGELSGSMTMVLVSFP-COOH
G1'-11'	NH ₂ -SGSMTMVLVSFP-COOH
G1'-7'	NH ₂ -TMVLVSFP-COOH
G1'-4'	NH ₂ -LSFP-COOH
G1'-19'amide	NH ₂ -GKRKPGELSGSMTMVLVSFP-CO-NH ₂
G2'-21'amide	NH ₂ -EEGKRKPGELSGSMTMVLVSFP-CO-NH ₂
E1'-19'	NH ₂ -QNLIAGPFSAATLVAASYS-COOH
F1'-19'	NH ₂ -GILNGGDFQTASMSMIYN-COOH
K1'-19'	NH ₂ -KSVVPGDYEAATFELTYR-COOH
H1'-19'	NH ₂ -KKLEAGNYFAVLGFRVDYE-COOH
MS	NH ₂ -YALAPNAV IPTSLALL-COOH

* Water insoluble

of seven COOH-terminal amino acids from a pilus subunit is sufficient for binding to PapD.

For further investigation of the role of the peptide's COOH-terminus in binding to PapD, the terminal proline was deleted and an amide was introduced to give peptide G2'-21' amide (Table 2). These modifications reduced the ability of the immobilized peptide to be recognized by PapD (Fig. 1B). In addition, the soluble G2'-21' amide was unable to inhibit PapD binding to the immobilized G1'-19' peptide (Fig. 1C). By contrast, formation of a COOH-terminal proline amide to create the peptide G1'-19' amide did not affect binding to PapD (Fig. 1, B and C). The COOH-terminal amino acid varies from pilus subunit to pilus subunit (Table 1). These data and the crystal structure described below indicate the importance of the COOH-terminal residue (not necessarily a proline) in binding to PapD.

Partial digestion with trypsin cleaved PapD in the F1-G1 loop at residue Lys⁹⁹ (Figs. 2A and 3, "T" site) (26). The rate of tryptic cleavage of PapD was reduced by prior incubation of PapD with the G1'-19', G1'-16', and K1'-19' peptides, but not with the G2'-21' amide peptide (Fig. 2A). In a similar experiment, native PapG protected PapD from proteolysis (27). The observed protection of PapD by bound peptides may be due to a change of the local conformation of the F1-G1 loop, or due to physical contact of the loop by the peptide, as suggested in a similar study of the chaperone SecB (5).

As previously described, native PapD is able to bind to reduced, denatured PapG and restore the PapD-PapG complex in vitro in a reconstitution assay (15). This assay has been proposed to reflect the recognition function of PapD in vivo (15) and was used to determine the ability of the peptides to inhibit PapD binding to PapG in vitro. We found that increasing amounts

of the G1'-19', G1'-16', and K1'-19' peptides inhibited restoration of the PapD-PapG complex by PapD, but that the G2'-

21' amide peptide had no effect (Fig. 2B). The ability of the PapG and PapK peptides to prevent PapD from binding to PapG

Table 3. Crystals of the PapD-peptide complex were obtained by vapor diffusion against 20 percent PEG8000, 0.1 M cacodylate buffer (pH 5.0), and 0.2 M calcium acetate. The crystallization drop contained equal volumes of reservoir and protein solution. The protein solution (17 mg/ml) consisted of a 1:1 molar ratio of PapD to peptide in 20 mM 2-[N-morpholino]ethanesulfonic acid (MES, Sigma) (pH 6.5) with 1.0 percent β -octyl glucoside. The crystals have two molecules in the asymmetric unit and diffracted to 2.9 Å resolution on a laboratory x-ray source. Intensity data were collected on a Xuong-Hamlin multiwire area-detector system (50). All data were obtained from a single crystal and were processed initially with MADNES (51). The data were merged and scaled with the use of ROTAVATA and AGROVATA from the CCP4 package (52). The structure of the complex was solved by molecular replacement with the program XPLOR (53). The search model used was the refined 2.0 Å resolution structure of PapD (19). The self-rotation function obtained from the data at 8.0 to 4.0 Å resolution gave a clear noncrystallographic twofold axis. The top two peaks of the cross-rotation function were related by the noncrystallographic twofold axis and subsequently gave the correct solution. The Patterson correlation (PC) refinement (54) was not required to solve the rotation function; when used, however, it did significantly improve the scores of the correct orientations over the background peaks. The PC refined solutions were then used in the translation functions where the top peaks in each search gave the correct position. After the translation functions the *R* factor was 39.0 percent for 8.0 to 4.0 Å resolution data. Subsequent rigid body refinement in which all four domains of the two PapD molecules in the asymmetric unit were allowed to refine independently resulted in an *R* factor of 36.4 percent for the same data. Examination of an $|F_o - F_c|$ electron density map at this stage with the graphics program O (55) showed clear density corresponding to the peptide in the PapD cleft and running along the surface of the protein. The orientation of the peptide was determined from the electron density, but initially only the final 10 COOH-terminal amino acids of the peptide could be modeled into density. Simulated annealing and atomic positional refinement with XPLOR was initiated at this stage. Noncrystallographic restraints were applied throughout the refinement procedure. Several additional cycles of model building and refinement were performed with four further peptide amino acids being added to yield an *R* factor for the current model of 18.2 percent for 8.0 to 3.0 Å resolution data. The model at the present refinement (which contains no water molecules and does not include the first five NH₂-terminal amino acids of the peptide) has root-mean-square (rms) deviations from ideal geometry of 0.020 Å for bonds lengths and 4.2° for bond angles.

Crystal data		Refinement parameters	
Space group	C2	Protein atoms	3,658
Unit cell (Å)		Δ bond (Å)	0.020
<i>a</i>	130.7	Δ angle (degrees)	4.2
<i>b</i>	83.5	Resolution (Å)	8.0-3.0
<i>c</i>	59.2	Reflections	9,592
β	117.2°	<i>R</i> _{cryst} †	0.182
Resolution (Å)	3.0		
Total measurements	32,684		
Unique reflections	11,407		
Percent complete 20-3.0 Å	83.2		
Percent complete 3.2-3.0 Å	72.1		
<i>R</i> _{sym} *	0.68		

* $R_{sym} = \sum |I_{hi}| - I_{hi} / \sum I_{hi}$, where I_{hi} and I_h are the intensities of the individual and mean structure factors, respectively. † $R_{cryst} = \sum |F_{obs}| - |F_{calc}| / \sum F_{obs}$. Only data with $F_{obs}/\sigma(F_{obs}) > 2.0$ were used in the refinement.

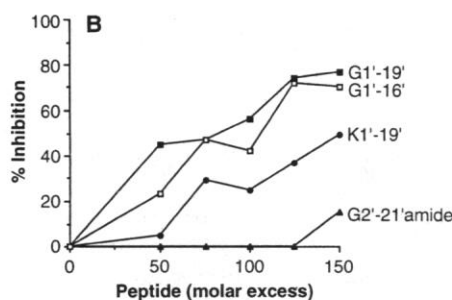
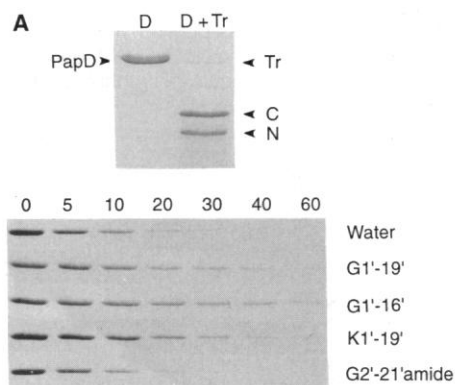


Fig. 2. Binding of pilus subunit-related peptides to PapD provides protection against enzymatic proteolysis and blocks binding of PapD to PapG. (A) Upper PapD (15 μ g) was incubated with PBS (lane D) or with 1.5 μ g of trypsin (lane D+Tr) at 37°C for 20 minutes and applied to 20 percent SDS-PAGE. Coomassie blue-stained bands corresponding to full-length PapD (PapD), trypsin (Tr), the NH₂-terminal fragment of PapD (N), and the COOH-terminal fragment of PapD starting at residue 100 (C) (26) are indicated. (Lower) PapD incubated

with 20-times molar excess of peptides G1'-19', G1'-16', K1'-19', or G2'-21' amide, or an equivalent volume of water, was digested with trypsin and applied to 15 percent SDS-PAGE and Coomassie-stained (56). Bands corresponding to full-length PapD remaining after 0, 5, 10, 20, 30, 40, and 60 minutes of digestion are shown. (B) PapD that had been incubated with the G1'-19', G1'-16', K1'-19', or G2'-21' amide peptides was added to reduced, denatured PapD-PapG, and the amount of PapD-PapG restored in each sample was quantitated as described (57). The percent inhibition represents the relative decrease in the amount of the PapD-PapG complex restored with peptide-treated PapD compared with the amount of PapD-PapG complex restored with untreated PapD. The graph represents the average of four experiments.

indicated that these peptides bound similarly to PapD and that they occupied the pilus subunit binding site of PapD.

Crystal structure of the PapD-PapG peptide complex. In order to gain insight into the structural basis of the recognition function of PapD and also to facilitate the design of synthetic PapD inhibitors which could act as antibacterial agents, the crystal structure of the complex between PapD and the peptide G1'–19' was determined and

refined to 3.0 Å resolution (Table 3). The peptide bound in an extended conformation with its COOH-terminal residue (Pro^{1'}) anchored within the interdomain cleft (Figs. 3 and 4). The peptide was anchored in the cleft by hydrogen bonds formed between the COOH-terminus of the peptide and Arg⁸ and Lys¹¹² which are invariant (7, 10) among all members of the periplasmic chaperone family (Figs. 3 and 4). The current electron density maps at

3.0 Å resolution did not allow us to determine whether the guanidino group of Arg⁸ formed one or two hydrogen bonds with the Pro^{1'} carboxyl group. However, the former hydrogen bonding arrangement and the indication from the electron density that both the guanidino group and the peptide COOH-terminus may be partially solvated was consistent with the observation that amidation of G1'–19' did not result in decreased binding to PapD (Fig. 1, B and C). Thus, the importance of the charge of the COOH-terminus to peptide binding is still uncertain. The Pro^{1'} side chain made van der Waals contacts in the cleft with residues from both domains of PapD: Thr⁷, Thr¹⁵², Ile¹⁵⁴, Thr¹⁷⁰, and Ile¹⁹⁴. The neighboring peptide residue, Phe^{2'}, which is highly conserved as Tyr in the other pilus subunits (Table 1), was positioned in a shallow pocket formed between the two β sheets of the NH₂-terminal domain of PapD. The residues Leu⁴, Thr⁷, Thr¹⁰⁹, and Ile¹¹¹ that line the pocket and make hydrophobic interactions with Phe^{2'} are all highly conserved in the periplasmic chaperone family (7, 10). Along the surface of the NH₂-terminal domain, the peptide forms a parallel β-strand interaction with strand G1. In this way, seven main chain hydrogen bonds were formed between Met^{8'} to Phe^{2'} of the peptide and Gln¹⁰⁴ to Lys¹¹⁰ of PapD, thus extending the β sheet of PapD out into the peptide (Fig. 3 and Table 4).

In addition to the COOH-terminal residues Pro^{1'} and Phe^{2'}, only Leu^{4'}, Met^{6'}, and Met^{8'} in the peptide made significant contacts with PapD. Residues Met^{6'} and Met^{8'} interacted with Leu¹⁰³, Ile¹⁰⁵, and Leu¹⁰⁷ of strand G1. Together with Phe^{2'}, and Leu^{4'}, Met^{6'} and Met^{8'} are part of the conserved pattern of alternating hydrophobic and hydrophilic residues in the COOH-termini of the pilus subunits (Table 1). Similarly, PapD residues Leu¹⁰³, Ile¹⁰⁵, and Leu¹⁰⁷ compose a conserved pattern of hydrophobic residues in the periplasmic chaperone family (7, 10). Our calculations revealed that the four hydrophobic peptide side chains of residues 2', 4', 6', and 8' contribute 20 percent of the total buried surface area (582 Å²) between the peptide and protein. Therefore even though the major stabilization of the complex is provided by hydrogen bonding, hydrophobic interactions are not insignificant, and we propose that they provide part of the explanation for the specificity of PapD for pilus related peptides and subunits. Experimental support of this theory is provided by the reduced binding of PapD to the peptide G2'–21' amide as compared to the G1'–19' peptide (Fig. 1, B and C). Hydrogen bonding of the COOH-terminus of the G2'–21' amide (which lacks Pro^{1'}) to Arg⁸ and Lys¹¹² of PapD would allow main chain

Fig. 3. Model of the three-dimensional structure of PapD co-crystallized with the G1'–19' peptide, determined to 3.0 Å resolution. The peptide bound in an extended conformation along the G1 β strand in the cleft of PapD and the terminal carboxylate group (highlighted in white) formed hydrogen bonds with residues Arg⁸ (R8) and Lys¹¹² (K112) of PapD (highlighted in yellow and orange, respectively). Hydrogen bonds between main chain atoms are depicted as white lines. PapD residues Glu¹⁶⁷ (E167) and Thr⁷ (T7) are shown in violet and dark blue, respectively. Conserved hydrophobic residues at positions 2, 4, 6, 8, and 12 from the COOH-terminus of the peptide are highlighted in red on the peptide chain shown in light blue. The conserved series of hydrophobic residues, 103, 105, 107, found in all members of the periplasmic chaperone family (7) are highlighted in green on the PapD ribbon (violet). The site of tryptic (T) cleavage is indicated.

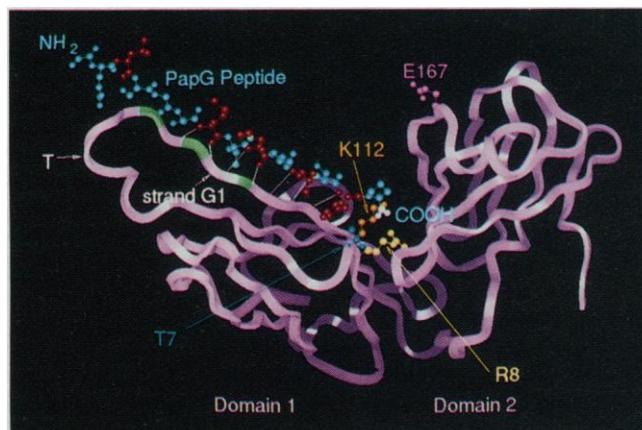


Table 4. Hydrogen bond interactions between PapD the bound G1'–19' peptide (PapD₁ and peptide₁) and its noncrystallographically related complex (PapD₂ and peptide₂). Hydrogen bonds are indicated by ·····. In the current 3.0 Å resolution model the distance (3.2 to 3.7 Å) and geometry between some of the groups are incompatible with efficient hydrogen bonding (as indicated by the question marks).

PapD ₁	Peptide ₁	Peptide ₂	PapD ₂
		Pro ^{1'} COOH·····Arg ⁸ NH ₂	
		Pro ^{1'} COOH·····Lys ¹¹² NZ	
		Phe ^{2'} NH·····Lys ¹¹⁰ C=O	
	Glu ^{13'} NH·····Ser ^{3'} C=O		
	Glu ^{13'} C=O·····Ser ^{3'} NH		
		Leu ^{4'} C=O·····Lys ¹¹⁰ NH	
		Leu ^{4'} NH·····Gln ¹⁰⁸ C=O	
	Ser ^{11'} NH·····Val ^{5'} C=O		
	Ser ^{11'} C=O·····Val ^{5'} NH		
		Met ^{6'} C=O·····Gln ¹⁰⁸ NH	
		Met ^{6'} NH·····Ala ¹⁰⁶ C=O	
	Ser ^{9'} NH·····?·····Thr ⁷ C=O		
	Ser ^{9'} C=O·····?·····Thr ⁷ NH		
Gln ¹⁰⁴ C=O·····Met ^{8'} NH		Met ^{8'} C=O·····Ala ¹⁰⁶ NH	
Ala ¹⁰⁶ NH·····Met ^{8'} C=O		Met ^{8'} NH·····Gln ¹⁰⁴ C=O	
	Thr ⁷ NH·····?·····Ser ^{9'} C=O		
	Thr ⁷ C=O·····?·····Ser ^{9'} NH		
Ala ¹⁰⁶ C=O·····Met ^{6'} NH			
Gln ¹⁰⁸ NH·····Met ^{6'} C=O			
	Val ^{5'} NH·····Ser ^{11'} C=O		
	Val ^{5'} C=O·····Ser ^{11'} NH		
Ala ¹⁰⁶ C=O·····Leu ^{4'} NH			
Lys ¹¹⁰ NH·····Leu ^{4'} C=O			
	Ser ^{3'} NH·····Glu ^{13'} C=O		
	Ser ^{3'} C=O·····Glu ^{13'} NH		
Lys ¹¹⁰ C=O·····Phe ^{2'} NH			
Lys ¹¹² NZ·····Pro ^{1'} COOH			
Arg ⁸ NH ₂ ·····Pro ^{1'} COOH			

hydrogen bonding but would then dislocate the four hydrophobic side chains in the peptide from their subsites in PapD, resulting in a reduction in binding strength.

Within the crystal, the PapD-peptide β sheet was extended even further as a result of noncrystallographic twofold symmetry that placed a second PapD-peptide complex adjacent to the first so that the two bound peptide chains interacted as antiparallel β strands. In our model, eight main chain hydrogen bonds are formed between the two peptides (Table 4). A mixed β sheet is thus created between the two complexes and extends over 10 β strands (Fig. 5). No contacts were observed between the two noncrystallographically related PapD molecules themselves, both of which were positioned in similar environments within the crystal and had a similar number of intermolecular contacts. The calculated buried surface area between the two noncrystallographically related peptides was 520 \AA^2 , a value similar to the surface area buried between the protein and peptide. This dimerization appears to be a consequence of crystal packing because all evidence shows that PapD forms monomeric complexes with peptides or with intact PapG in solution.

The hydrogen bonding pattern between PapD and the peptide broke at Ser^{9'} but the peptide remained in van der Waals contact with PapD until Ser^{11'} where the peptide ran beyond the F1-G1 loop but remained hydrogen-bonded to the noncrystallographically related peptide as far as Glu^{13'} (Table 4). The last resolved amino acid of the peptide was Gly^{14'} which was positioned close to the binding cleft of the noncrystallographically related PapD. The first five NH₂-terminal amino acids, including three positively charged residues, showed no density and therefore must have been disordered in the crystal structure. In agreement with this, the NH₂-terminus of the peptide was not important for binding to PapD in solution because the G1'-7' peptide lacking the NH₂-terminal 12 amino acids effectively inhibited PapD binding to the immobilized G1'-19' peptide (Fig. 1C).

The structures of the individual PapD domains in the peptide complex were essentially the same as those of native PapD (18, 19). However, there was a significant movement of the domains with respect to each other with a 13° jaw-closing or hinge-bending motion making the angle of the PapD boomerang more acute (Fig. 6). Whether or not this conformational difference between the two crystal structures was due to peptide binding or crystal packing is still unclear.

In the native PapD structure, the electron density obtained for the long F1-G1 loop was poor between residues 96 and 102, suggesting that it was rather flexible and

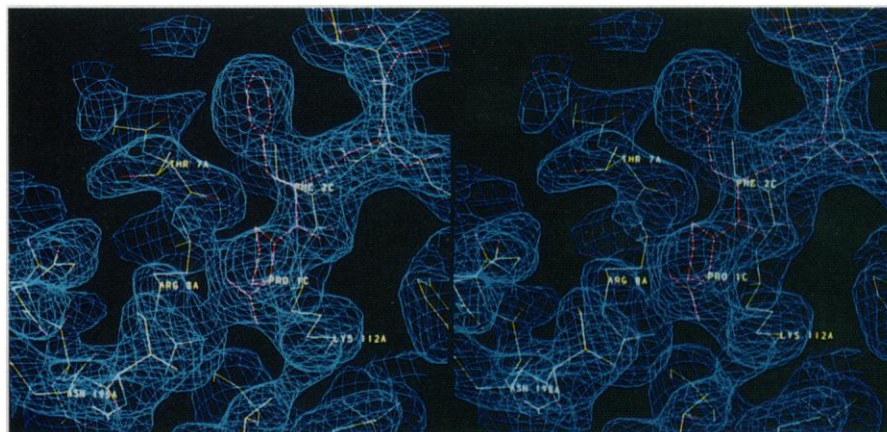


Fig. 4. Stereoscopic view of the 3.0 \AA resolution electron density of the G1'-19' peptide COOH-terminus (purple) and neighboring PapD residues, superimposed on the refined structure. The electron density map (blue) was calculated with coefficients $(2|F_o| - |F_c|)$ and contoured at 1σ .

disordered in the crystal (19). In the peptide complex, however, this loop was better resolved, indicating that binding of the peptide made this loop more rigid. Superimposing the NH₂-terminal domains of native PapD and the peptide complex showed a significant difference in the F1-G1 loop position between the two structures (rms for the 110 NH₂-terminal C α atoms is 1.84 \AA , with a maximum main chain movement of about 9 \AA for Leu¹⁰³). In the peptide complex, one end of the loop twisted away from the β barrel of the NH₂-terminal domain, thus facilitating a more extensive contact between strand G1 and the peptide. As with the hinge-bending of the two domains, it is not yet possible to say with certainty whether this loop shift was a consequence of peptide binding or of crystal packing; the rather open conformation of the F1-G1 loop suggests that it may be largely the latter. Nevertheless, evidence that similar interactions between PapD and peptides or pilus subunits occur in solution was provided by protease protection exper-

iments where the F1-G1 loop of PapD was protected from tryptic cleavage by the binding of both native PapG (27) and the G1'-19' peptide (Fig. 2A).

A molecular anchor in the chaperone cleft. Site-directed mutations were constructed in PapD to investigate whether the crystal structure of the PapD-peptide represented part of the PapD-pilus subunit interactions that are important in pilus assembly (Fig. 3). From the crystal data, the invariant residues Arg⁸ and Lys¹¹² in PapD formed hydrogen bonds to the COOH-terminus of the bound peptide. To evaluate the importance of these interactions, we changed Lys¹¹² to an alanine to remove the charged side chain and to a methionine to replace the charged group with a hydrophobic group while maintaining the side chain packing (28). Mutations of Arg⁸ to glycine, alanine, and methionine have been shown to abolish the ability of PapD to bind to subunits and mediate pilus assembly in vivo (20). The highly conserved Thr⁷ in PapD, which formed van der Waals and hydropho-

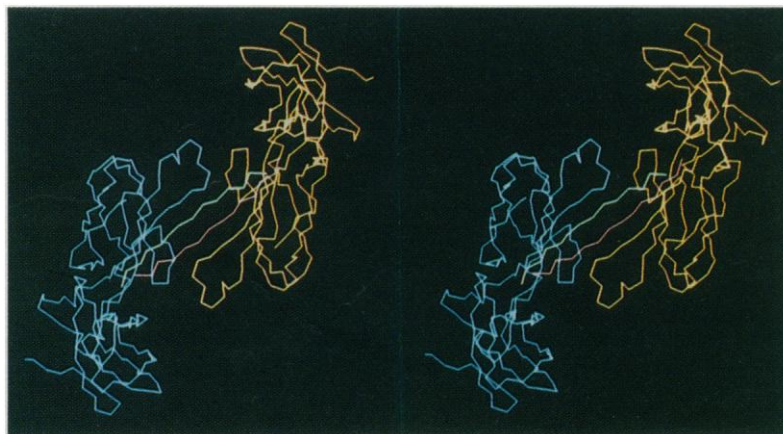


Fig. 5. Stereoscopic view of a PapD-peptide complex (PapD, yellow; peptide, red) showing its interaction with a twofold noncrystallographically related complex (PapD, blue; peptide, green).

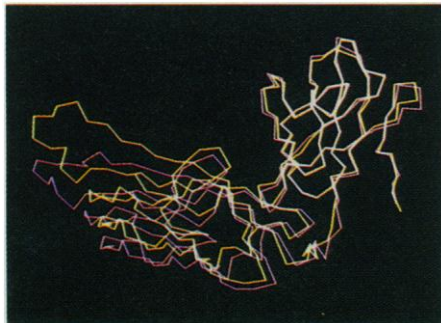


Fig. 6. Superposition of COOH-terminal domains of native PapD (magenta) and complexed PapD (yellow). The two structures have been superimposed using the LSQ option in the program O (55). The resulting rms for 98 C α atoms of the COOH-terminal domain was 0.66 Å.

bic interactions with the peptide in the crystal structure, was changed to a valine (28). This mutation maintained the steric volume of the side chain and allowed an evaluation of whether the hydroxyl group formed critical hydrogen bonds to the subunits. Glu¹⁶⁷ is a variable residue in domain 2 of PapD which was distant from the bound peptide and therefore less likely to be important for subunit binding and pilus assembly. Radical Glu¹⁶⁷ mutations to histidine, aspartic acid, threonine, and glycine have all been shown to have little or no effect on PapD function in vivo (20). All of the mutants described above were secreted into the periplasmic space as stable proteins similar to wild-type PapD. In addition, the elution profiles from a cation-exchange high-performance liquid chromatography (FPLC®, Pharmacia) column and the electrophoretic properties of the purified mutant PapDs were similar to the wild-type protein, supporting the prediction that these mutations would not affect

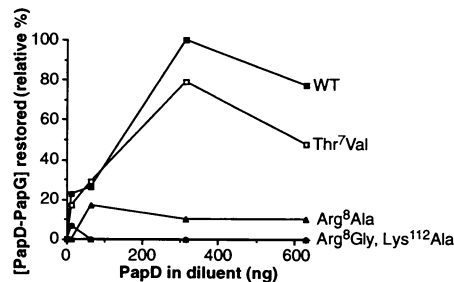


Fig. 7. Ability of PapD Arg⁸, Lys¹¹², and Thr⁷ mutants to bind PapG and restore the PapG-PapD complex in vitro. PapD-PapG complex (0.4 μg) was reduced and denatured as described in Fig. 2B. The denatured PapD-PapG complex was then diluted with 0 to 630 ng of purified wild-type (WT) or mutant PapD. The amount of PapD-PapG restored in the samples was determined as described in Fig. 2B and was graphed as a percentage of the greatest amount of PapD-PapG restored, averaged for three experiments.

the overall structure of PapD (28).

Mutations in Arg⁸ and Lys¹¹² abolished the ability of PapD to bind to denatured PapG and reconstitute the PapD-PapG complex in vitro, whereas the mutation in Thr⁷ had little or no effect on PapD-PapG interactions in vitro (Fig. 7). Similarly, mutations in Arg⁸ and Lys¹¹² abolished the ability of PapD to bind to pilus subunits and mediate pilus assembly in vivo, but mutations in Thr⁷ and Glu¹⁶⁷ had little or no effect on PapD function in vivo (Table 5). These studies revealed that the invariant Arg⁸ and Lys¹¹² residues predicted to be critical for peptide binding in the PapD-peptide crystal were also essential for PapD function in mediating pilus subunit binding and assembly in vivo.

A molecular zipper between chaperone and pilus protein. In the crystal, the peptide G1'-19' anchored in the cleft of PapD

via its COOH-terminus and it then extended along the G1 β strand toward the F1-G1 loop. The argument that the structure of the complex was significantly influenced by crystal packing interactions and thus might not reflect the situation in vivo was refuted by both in vitro and in vivo data. Peptide binding protected the F1-G1 loop from protease cleavage, and cleft residues Arg⁸ and Lys¹¹² were critical for binding PapG in vitro and for PapD-subunit interactions in pilus assembly in vivo. Therefore the interactions found in the crystal structure of the complex between PapD and the G1'-19' peptide probably reflect an important part of the interface between PapD and the pilus subunit.

The molecular interactions between PapD and the peptide illustrate a mechanism of general relevance to chaperone binding of target proteins. PapD residues Arg⁸ and Lys¹¹² protrude into the cleft between the two domains of the chaperone and probably serve as a molecular anchor for the COOH-terminus of pilus proteins. Both Arg⁸ and Lys¹¹² are invariant among periplasmic chaperones, indicating that they are likely to have a universal role in anchoring the COOH-terminus of pilus subunits in the other PapD-like chaperone listed in Table 1. Backbone hydrogen bonds along the G1 β strand of the chaperone subsequently provide strong zippering interactions along the length of the COOH-terminus of the subunit and allow binding to a number of polypeptides in a relatively sequence-independent manner. However, it is clear that the binding does not rely solely on backbone hydrogen bonds, since PapD does not bind randomly to peptides in vitro, or proteins in vivo. Part of the specificity in binding between PapD and pilus subunits seems to be due to the alternating pattern of hydrophobic and hydrophilic residues in the COOH-terminus and their spacing with the terminal carboxylate group of the pilus subunits. Another layer of specificity may come from other contacts between the chaperone and the subunit and may occur after the COOH-terminus has anchored into the chaperone cleft. Variable residues in loop regions of antibodies provide the exquisite specificity necessary for an extensive antibody binding repertoire (29). Similarly, residues in the F1-G1 loop of PapD and other variable loops at the tips of both domains may provide further specificity to chaperone binding since these have been found to vary in length and composition amongst members of the periplasmic chaperone family (7, 10). In addition, other regions of pilus subunits may be involved in chaperone binding, such as conserved NH₂-terminal sequences in the pilus subunits (21).

The mode of peptide binding to PapD is

Table 5. Effects of mutations on PapD function in vivo.

Residue class	Mutation	HA titer*	Pilus assembly†	Subunit stabilization‡				
				PapA	PapE	PapG	PapF	PapK
Invariant	Arg ⁸ Gly	None	-	-	-	-	-	-
	Arg ⁸ Ala	None	-	+	-	+	-	+
	Arg ⁸ Met	None	-	++	-	++	-	++
	Lys ¹¹² Ala	None	-	+	-	+	-	+
	Lys ¹¹² Met	None	-	++	-	-	-	-
Conserved	Thr ⁷ Val	64	+++	++++	++++	++++	++++	++++
Variable	Glu ¹⁶⁷ X§	128	++++	++++	ND	ND	++++	++++

*The *E. coli* strain HB101 containing plasmid pPAP37 (which encodes all of the *pap* genes except *papD*) (8) was complemented with wild-type and mutant *papD*-encoding plasmids (28) to determine the effect of the mutations on hemagglutination (HA) titer and pilus assembly. The HA titer was quantitated (20) after induction with 0.01 mM isopropyl-β-D-thiogalactopyranoside (IPTG). The HA titer represents the greatest bacterial dilution that still agglutinates erythrocytes, HB101/pPAP37 expressing wild-type PapD has an HA titer of 128. †The amount of pili assembled on the cells was quantitated (20) after induction with 0.01 mM IPTG. (-) No pili were detected; (+) relative degree of piliation; and the degree of piliation of HB101/pPAP37 expressing wild-type PapD corresponds to + + + +. ‡Chaperone-assisted periplasmic stabilization of pilus subunits PapA, PapE, PapF, PapK, and PapG was determined by immunoblotting of periplasmic extracts as described (20). (-) No stabilization of the subunit; (+) the degree of subunit stabilization; wild-type PapD stabilization corresponds to + + + +; and (ND) not done. §X indicates mutations to His, Asp, Thr, or Gly.

similar to the binding of the streptococcal protein G to a Fab fragment, in which an outer β strand on the protein G domain formed an antiparallel interaction with the last strand in the constant heavy domain of the Fab and extended out the β sheet into protein G (30). The major difference between the two complexes is that the peptide bound to PapD in a parallel manner rather than an antiparallel one. The interactions between G1'-19' and PapD, like the protein G-Fab complex, therefore represent a binding paradigm for β -barrel motif proteins distinct from antibody-antigen and growth hormone-growth hormone receptor interactions (29, 31). Unlike the protein G-Fab complex, however, PapD utilizes residues in the interdomain cleft of its immunoglobulin-like structure to bind to several different proteins.

Chaperone-subunit interactions are a fundamental step in the cascade of protein-protein interactions that eventually lead to pilus assembly and presentation of virulence-associated adhesins on the bacterial surface. The PapD-peptide crystal structure is the first to date illustrating a mechanism by which chaperones may interact with their target proteins. The agreement between crystallography, mutagenesis, and experiments with purified proteins and peptides suggests that the mode of chaperone binding described in this article actually presents a "snapshot" of a process fundamental to Gram-negative pathogens. The molecular details of the chaperone-adhesin interaction and optimization of the minimum inhibitory heptamer peptide with synthetic peptide libraries (32) may lead to the design of high affinity synthetic inhibitors which would prevent pilus assembly by binding in the chaperone cleft. The conserved nature of the chaperone-subunit interaction may make such inhibitors effective against various Gram-negative pathogens.

REFERENCES AND NOTES

- M.-J. Gething and J. Sambrook, *Nature* **355**, 33 (1992).
- S. J. Landry, R. Jordan, R. McMacken, L. M. Gierasch, *ibid.*, p. 455.
- S. J. Landry and L. M. Gierasch, *Biochemistry* **30**, 7359 (1991).
- G. C. Flynn, J. Pohl, M. T. Flocco, J. E. Rothman, *Nature* **353**, 726 (1991).
- L. L. Randall, *Science* **257**, 241 (1992).
- S. J. Hultgren *et al.*, *Cell* **73**, 887 (1993).
- A. Holmgren, M. J. Kuehn, C.-I. Branden, S. J. Hultgren, *EMBO J.* **11**, 1617 (1992).
- F. Lindberg, J. M. Tennent, S. J. Hultgren, B. Lund, S. Normark, *J. Bacteriol.* **171**, 6052 (1989).
- C. H. Jones *et al.*, *Proc. Natl. Acad. Sci. U.S.A.* **90**, 8397 (1993).
- F. Jacob-Dubuisson, M. J. Kuehn, S. J. Hultgren, *Trends Microbiol.* **1**, 50 (1993).
- M. J. Kuehn, J. Heuser, S. Normark, S. J. Hultgren, *Nature* **356**, 252 (1992).
- F. Jacob-Dubuisson, J. Heuser, K. Dodson, S. Normark, S. J. Hultgren, *EMBO J.* **12**, 837 (1993).
- M. Gong and L. Makowski, *J. Mol. Biol.* **228**, 735 (1992).
- M. Baga, M. Norgren, S. Normark, *Cell* **49**, 241 (1987).
- M. J. Kuehn, S. Normark, S. J. Hultgren, *Proc. Natl. Acad. Sci. U.S.A.* **88**, 10586 (1991).
- S. J. Hultgren *et al.*, *ibid.* **86**, 4357 (1989).
- K. Dodson, F. Jacob-Dubuisson, R. T. Striker, S. J. Hultgren, *ibid.* **90**, 3670 (1993).
- A. Holmgren and C. I. Branden, *Nature* **342**, 248 (1989).
- A. Holmgren and D. J. Ogg, in preparation.
- L. Slonim, J. Pinkner, C.-I. Branden, S. Hultgren, *EMBO J.* **11**, 4747 (1992).
- S. Normark *et al.*, in *Microbial Lectins and Agglutinins: Properties and Biological Activity*, D. Mirelman, Ed. (Wiley, New York, 1986), pp. 113-143.
- B. L. Simons *et al.*, *FEMS Microbiol. Lett.* **67**, 107 (1990).
- The peptides were synthesized with the 9-fluorenylmethoxycarbonyl (Fmoc)-solid-phase strategy and then purified (>95 percent) by reversed-phase high-performance liquid chromatography (HPLC); peptide structures were confirmed by fast atom bombardment mass spectroscopy and amino acid analysis (K. Flemmer, S. Roy, B. Walse, J. Kihlberg, in preparation).
- PapD-immobilized peptide ELISA: Stock solutions of peptides (5 mg/ml) in water or 50 percent acetic acid were diluted to a concentration of 2.5 pmol per 50 μ l in phosphate-buffered saline (PBS) (120 mM NaCl, 2.7 mM KCl, 10 mM PBS, pH 7.4). A portion (50 μ l) of the peptide solution was coated overnight onto microtiter wells (Nunc-Immuno Plate Maxisorp) at 4°C. The solutions in the plates were discarded, and the wells were blocked with 200 μ l of 3 percent bovine serum albumin (BSA, Sigma) in PBS for 2 hours at 25°C. The plates were washed vigorously three times with PBS and incubated with 50 μ l of the indicated amount of purified PapD (8). After three washings with PBS, the wells were incubated with a 1:500 dilution of rabbit antiserum to PapD (8) in 3 percent BSA-PBS for 45 minutes at 25°C. After three washings with PBS, the wells were incubated with a 1:1000 dilution of goat antiserum to rabbit IgG (immunoglobulin G) coupled to alkaline phosphatase (Sigma) in 3 percent BSA-PBS for 45 minutes at 25°C. After three washings with PBS and three washings with developing buffer (10 mM diethanolamine, pH 9.5, 0.5 mM MgCl₂), 50 μ l of filtered *p*-nitrophenyl phosphate substrate (10 mg/ml, Sigma) in developing buffer was added; the reaction was incubated for 60 minutes in the dark at 25°C, and the absorbance at 405 nm was read.
- PapD-peptide inhibition ELISA: Microtiter wells were coated overnight at 4°C with 50 μ l of the G1'-19' peptide at 2.5 pmol/50 μ l in PBS. The wells were washed with PBS and blocked with 3 percent BSA. Each test peptide (2.5 nmol) was incubated with 100 pmol of PapD for 30 minutes, and the PapD-peptide solution was then added to the coated wells and incubated at 25°C for 45 minutes in the presence of 3 percent BSA-PBS. The subsequent primary antibody, secondary antibody, and developing steps have been described (24). The ability of the peptides to inhibit binding of PapD to the G1'-19' peptide was calculated by dividing the amount of PapD binding in the presence of peptide with the amount of PapD binding in the presence of water and subtracting the value from 1. No inhibition (0 percent) includes values where binding was greater than that of PapD when incubated with water alone.
- PapD (400 μ g) was partially digested by incubation with 4.5 μ g of trypsin in PBS for 20 minutes at 37°C. The PapD digests were applied to a C-18 HPLC column (Beckman) and two major fragments were eluted with a 0 to 100 percent acetonitrile gradient in 0.01 percent trifluoroacetic acid. The NH₂-terminal amino acid sequence of the approximately 14-kD tryptic fragment was identified as residues 100-108, corresponding to cleavage after Lys⁹⁹, and the NH₂-terminal sequence of the 11-kD bands in the trypsin digest was identical to the NH₂-terminal sequence of PapD.
- M. Kuehn and S. Hultgren, unpublished data.
- Site-directed mutagenesis was performed with the Bio-Rad in vitro mutagenesis kit. The following primers (noncoding strand) were used to introduce mutations in the *papD* gene:
T7V, 5'-GTCAAACACCGCCGGAAGCTGTCCAGCGA-3';
K112A, 5'-CGGGCATAAAAAAGAGCTATTTTGGTCTG-3';
K112M, 5'-CGGATAAAAAAGCATTATTTTCTCTG-3'.
Mutations in *papD* were confirmed by sequencing, and the altered *papD* genes were cloned into vector pMMB91 under the inducible P_{tac} promoter as described for other *papD* mutations (20). The resulting plasmids, pT7V, pK112A, and pK112M, encode PapD with point mutations changing Thr⁷ to Val, and Lys¹¹² to Ala and to Met, respectively. Plasmid pLS101 is an isogenic construct containing the wild-type *papD* gene; plasmids pE167H, pE167D, pE167T, and pE167G encode PapD with point mutations changing Glu¹⁶⁷ to His, Asp, Thr and Gly, respectively; and plasmids pR8G, pR8A, and pR8M encode PapD with point mutations changing Arg⁸ to Gly, Ala, and Met, respectively (20). Mutant PapDs were purified [L. Slonim, thesis, Washington University (1993)] by the method described for purification of wild-type PapD (8).
- D. R. Davis, E. A. Padlan, S. Sheriff, *Annu. Rev. Biochem.* **59**, 439 (1990); A. F. Williams and A. N. Barclay, *Annu. Rev. Immunol.* **6**, 381 (1988).
- J. P. Derrick and D. B. Wigley, *Nature* **359**, 752 (1992).
- A. M. de Vos, M. Ultsch, A. A. Kossiakoff, *Science* **255**, 306 (1992).
- K. S. Lam *et al.*, *Nature* **354**, 82 (1991); R. A. Houghten *et al.*, *ibid.*, p. 84.
- B.-I. Marklund *et al.*, *Mol. Microbiol.* **6**, 2225 (1992).
- T. Schmolli *et al.*, *ibid.* **3**, 1735 (1989).
- T. Schmolli, J. Hacker, G. Werner, *FEMS Microbiol. Lett.* **41**, 229 (1987).
- P. Klemm and G. Christiansen, *Mol. Gen. Genet.* **208**, 439 (1987).
- P. E. Orndorff and S. Falkow, *J. Bacteriol.* **163**, 454 (1985).
- W. Gaastra and F. K. de Graaf, *FEMS Microbiol. Lett.* **22**, 253 (1984).
- P. Lintermans, thesis, Rijksuniversiteit Ghent, (1990).
- P. Lintermans *et al.*, *Infect. Immun.* **56**, 1475 (1988).
- W. Gaastra, F. R. Mooi, A. R. Stuitje, F. K. de Graaf, *FEMS Microbiol. Lett.* **12**, 41 (1981).
- M. B. Jalajakumari, C. J. Thomas, R. Halter, P. A. Manning, *Mol. Microbiol.* **3**, 1685 (1989).
- B. Roosendaal, G.-F. Gerlach, S. Clegg, B. Allen, *J. Bacteriol.* **171**, 1262 (1989).
- B. L. Allen, G.-F. Gerlach, S. F. Clegg, *ibid.* **173**, 916 (1991).
- J. R. Gilsdorf, C. F. Marrs, K. W. McCrae, L. J. Forney, *Infect. Immun.* **58**, 1065 (1990).
- E. E. Galyov *et al.*, *FEMS Lett.* **286**, 79 (1991).
- I. Livey, C. J. Duggleby, A. Robinson, *Mol. Microbiol.* **1**, 203 (1987).
- F. R. Mooi, A. ter Avest, H. G. van der Heide, *FEMS Microbiol. Lett.* **54**, 327 (1990).
- S. C. Clouthier, K.-H. Muller, J. L. Doran, S. K. Collinson, W. W. Kay, *J. Bacteriol.* **175**, 2523 (1993).
- Department of Molecular Biology, Biomedical Center, Uppsala, Sweden; N.-H. Xuong, C. Neilson, R. Hamlin, D. J. Anderson, *J. Appl. Crystallogr.* **18**, 342 (1985).
- A. Messerschmit and J. W. Pflugrath, *J. Appl. Crystallogr.* **20**, 306 (1987).
- CCP4, The SERC (UK) Collaborative Project No. 4, A Suite of Programs for Protein Crystallography [Darebury Laboratory, Warrington WA4 4AD, United Kingdom (1979)].
- A. T. Brunger, X-PLOR Manual, Version 3.0 (Yale University, New Haven, CT, 1992).
- _____, *Acta Crystallogr.* **46**, 46 (1990).
- A. T. Jones and M. Kjeldgaard, O Version 5.6 (Department of Molecular Biology, Uppsala, Sweden, 1992).
- Purified PapD (50 μ g) was incubated for 15 minutes at 25°C with 20-times molar excess of G1'-19', G1'-16', K1'-19', or G2'-21' amide

peptides, or an equivalent volume of water. Each sample was then incubated at 37°C with 3.2 µg of trypsin (any trypsin cleavage sites in these peptides occur at their NH₂-termini, where they were predicted not to interfere with binding to PapD). Equivalent portions were removed after 0, 5, 10, 20, 30, 40, and 60 minutes and boiled in SDS-PAGE sample buffer to stop the digestion.

57. PapD and the PapD-PapG complex were purified as described (8, 16). Purified PapD-PapG complex (0.3 µg) (16) was reduced and denatured by

incubation at 25°C for 20 minutes with 4 M urea and 10 mM dithiothreitol. Purified PapD [1.2 µg (50 pmol)] (3) was incubated at 25°C for 10 minutes with 5 to 14.5 µg (2.5 to 7.25 nmol) of peptide. The PapD-peptide solution was then added to the reduced, denatured PapD-PapG, incubated at 25°C for 10 minutes, and applied to an IEF 3-9 gel (Pharmacia). The amount of PapD-PapG complex restored was quantitated by densitometry of the silver-stained IEF band corresponding to the pI of the PapD-PapG complex.

58. We thank J. Pinkner for purifying the PapD-PapG complex and the PapD mutants and S. Normark, C. Brändén, G. Magnusson, and S. Abraham for helpful advice and support. Supported by the Lucille P. Markey Charitable Trust and NIH grant R01AI29549 (S.J.H.), NIH training grant AI07172 (M.J.K.), and the Swedish National Board for Industrial and Technical Development (J.K. and K.F.).

13 April 1993; accepted 4 October 1993

AAAS–Newcomb Cleveland Prize

To Be Awarded for a Report, Research Article, or an Article Published in *Science*

The AAAS–Newcomb Cleveland Prize is awarded to the author of an outstanding paper published in *Science*. The value of the prize is \$5000; the winner also receives a bronze medal. The current competition period began with the 4 June 1993 issue and ends with the issue of 27 May 1994.

Reports, Research Articles, and Articles that include original research data, theories, or syntheses and are fundamental contributions to basic knowledge or technical achievements of far-reaching consequence are eligible for consideration for the prize. The paper must be a first-time publication of the author's own work. Reference to pertinent earlier work by the author may be included to give perspective.

Throughout the competition period, readers are

invited to nominate papers appearing in the Reports, Research Articles, or Articles sections. Nominations must be typed, and the following information provided: the title of the paper, issue in which it was published, author's name, and a brief statement of justification for nomination. Nominations should be submitted to the AAAS–Newcomb Cleveland Prize, AAAS, Room 924, 1333 H Street, NW, Washington, DC 20005, and **must be received on or before 30 June 1994**. Final selection will rest with a panel of distinguished scientists appointed by the editor of *Science*.

The award will be presented at the 1995 AAAS annual meeting. In cases of multiple authorship, the prize will be divided equally between or among the authors.